Superior stability and high capacity of restacked molybdenum disulfide as anode material for lithium ion batteries†

Guodong Du,[a] Zaiping Guo,*[ab] Shiquan Wang,[c] Rong Zeng,[a] Zhixin Chen[b] and Huakun Liu[a]

Received (in Cambridge, UK) 29th September 2009, Accepted 4th December 2009
First published as an Advance Article on the web 23rd December 2009
DOI: 10.1039/b920277c

Restacked MoS_2 with enlarged *c* lattice parameter and surface area was prepared by exfoliation and restacking process, exhibiting high reversible lithium storage capacity and superior rate capability as anode material for lithium ion batteries.

Lithium ion batteries have now become the main power sources for portable electronic devices. They have also attracted extensive attention as power sources for high power tools and electric vehicles, which require both high energy and high power density (high capacity and the ability to charge and discharge very fast). In order to meet the requirements of these new applications, electrode materials with high Li reversible storage capacity and fast Li^+ and electron transport are needed for lithium ion batteries.[1]

Layered transition-metal dichalcogenides MX_2 (M = Ti, Nb, Mo, Ta; X = S, Se, Te) are of great interest, as they act as host lattices by reacting with a variety of guest atoms or molecules to yield intercalation compounds, in which the guest is inserted between the host layers. In layered MX_2, atoms within a layer are bound by strong ionic/covalent forces, while the individual layers are bound by weak van der Waals interactions, forming a sandwich structure. MoS_2 is one of the most stable and versatile members of this family of layered materials. Three polytype crystal structures of MoS_2 have been reported so far,[2] as shown in ESI Fig. S1.† The lattice parameter *c* values for the 1T, 2H, and 3R polytypes are 6.147 Å, 12.294 Å, and 18.37 Å, respectively.[3–5]

Recently, it was reported that MoS_2 demonstrated reasonably reversible capacity ($\sim$400 mAh g^{-1}) and good cycling stability when used as anode material.[6] When a lithium ion first intercalates into these layered materials, it enters the S layer and forms Li–S bonds, resulting in volume changes. It was observed for TiS_2 that lattice parameter *c* suffers approximately 10% expansion, while the value of lattice parameter *a* remains almost the same associated to the intercalation process.[7,8] And for MoS_2, an increment to the *c* parameter of 0.25 Å was also reported for one mole of lithium intercalation.[9] In order to achieve high cycling stability, the stress induced by lithium intercalation/deintercalation cycling must be properly accommodated or relieved. It can be imagined that the increase of *c* lattice constant of MoS_2 can provide larger space for Li ion intercalation, which also reduces the barriers to Li ion mobility, thereby facilitating lithium ion diffusion.

Herein, we report on the exfoliation and restacking of layered MoS_2 with enlarged *c*-axis spacing for the first time and on the testing of the restacked MoS_2 as anode material for lithium ion batteries. Commercial raw MoS_2 was soaked in 1.5 equivalents butyllithium (*n*-BuLi, 1.6 M in hexane) and kept in argon atmosphere for a week. Then 0.1 g $LiMoS_2$ product was exfoliated in water into single layers through the redox reaction. The reactions are described as follows:[10]

$$MoS_2 + n\text{-BuLi} \rightarrow LiMoS_2 + 1/2C_8H_{18} \quad (1)$$

$$LiMoS_2 + H_2O \rightarrow (MoS_2)_{\text{exfoliated layers}} + LiOH + 1/2H_2 \quad (2)$$

The exfoliated MoS_2 is very sensitive to temperature. It will restack turbostratically when dried and it undergoes an irreversible phase transition to disordered 2H-MoS_2 at temperatures above 98 °C, and an ordered stacking appears at higher temperature.[11] Here, the restacking process was achieved *via* a hydrothermal procedure at 160 °C for 48 h.

The morphologies of the raw and the as-prepared restacked MoS_2 are shown in Fig. 1. The estimated *c*-axis parameter of the raw material is 0.620 nm and 0.635 nm for restacked MoS_2. The zone axis of the selected area electron diffraction (SAED) pattern of the inset in (a) is close to [100]. The normal of the stacked layers is parallel to [001]. In a direct comparison of raw and restacked MoS_2 in the top inset to (b), which shows nine layers, an obviously enlarged spacing for the restacked material can be seen. Fig. 1(c) shows the basal plane (001) of the restacked MoS_2, and the estimated plane spacing d_{100} is about 0.30 nm. The zone axis of the SAED pattern is [001], which shows a typical hexagonal structure. Fig. 1(d) shows a very clear *c* axis ordering with distortion and dislocation, indicating that the restacking of MoS_2 layers is turbostratic.

Both raw and restacked MoS_2 samples are single phase, as determined by the X-ray diffraction (XRD) patterns shown in Fig. 2. All reflections are in good agreement with a hexagonal structure (JCPDS No. 37-1492) which belongs to the space group $P6_3/mmc$ (No. 194). The raw material shows very sharp peaks with very high intensity, indicating good crystallization. The strong [002] peak (14.4°) signifies a well-stacked layered structure.[12] The restacked sample shows broadened peaks and a shortened [002] peak, which is consistent with previous reported restacked or partially exfoliated MoS_2,[13,14] suggesting that the mean crystallite size of the restacked MoS_2 is much smaller than that of the raw MoS_2. The broadened [00*l*] and

[a] *Institute for Superconducting and Electronic Materials, University of Wollongong, NSW 2522, Australia. E-mail: zguo@uow.edu.au; Fax: (+61) 2 4221 5731; Tel: +61 2 4221 5225*
[b] *School of Mechanical, Materials and Mechatronics Engineering, University of Wollongong, NSW 2522, Australia*
[c] *Department of Chemistry, Hubei University, Wuhan 430062, PR China*

† Electronic supplementary information (ESI) available: 1: Experimental characterization. 2: Crystal structure. 3: Raman spectra. 4: Magnetic measurements. 5: TEM and XRD of cycled restacked MoS_2. 6: EIS spectra. 7: Equivalent circuit. 8: Fitting line. 9: Calculated activation energy data. See DOI: 10.1039/b920277c

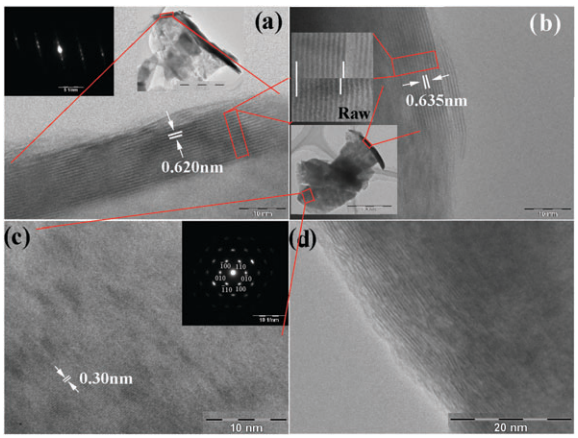

Fig. 1 Transmission electron microscope (TEM) images of raw and restacked MoS_2: (a) raw MoS_2, with the inset showing the corresponding SAED pattern; (b) restacked MoS_2, with the top inset showing a direct comparison of the layer spacing of raw and restacked MoS_2 by a comparison of 9 layers, while the bottom inset indicates the particle source of the images enlarged in (b) and (c); (c) restacked MoS_2, with the inset showing the corresponding SAED pattern; (d) turbostratically restacked MoS_2.

[10*l*] peaks also indicate a reduced number of layers along the *z*-axis perpendicular to the atomic layers in Fig. S1 (d).† The Rietveld refinement of the XRD pattern fits the experimental data well. The lattice parameters of the raw material can be determined to be $a = b = 3.159(1)$ Å, $c = 12.291(2)$ Å, which are in good agreement with the standard values cited previously. The corresponding parameters of the restacked MoS_2 are $a = b = 3.129(6)$ Å, $c = 12.526(8)$ Å (Bragg *R*-factor = 7.15, Rf-factor = 7.93). The great increase in the *c*-axis parameter of restacked MoS_2, by as much as 0.235 Å, indicates a larger space for lithium ions entering the S slab. On the other hand, the smaller size of the restacked MoS_2 compared to that of the raw material, might result in relaxation of the d spacing enlargement effect, resulting in improvements in the electrochemical stability of MoS_2. The Raman spectrum of the restacked MoS_2 is almost the same as that of the raw MoS_2 in the frequency range of 200 to 1000 cm^{-1}, confirming that the single layers of MoS_2 have restacked during hydrothermal process (ESI Fig. S2).†

In spite of their attractive capacity, none of the MoS_2 electrodes previously reported shows both high lithium storage and good capacity retention over the studied voltage range (0.01–3.0 V).[6,15,16] When MoS_2 is cycled between 3.0 and 0.01 V as an anode material, two step reactions occur. First, lithium intercalates into the S slab, and the van der Waals S–S bonds must be broken to be replaced by Li–S bonds. MoS_2 then decomposes into Mo nanoparticles embedded in a Li_2S matrix, corresponding to two cathodic peaks at about 1.0 V and 0.4 V in the first cathodic segment in the cyclic voltammograms (CVs), as shown in Fig. 3(a) and (b). Both the raw and the restacked samples show these two peaks. In the following cycles, an extra peak at about 2.0 V appears. This change can be explained by the formation of a gel-like polymeric layer.[6] *In situ* X-ray diffraction patterns have indicated that lithium intercalation at about 1.0 V corresponds to a phase change.[17] When lithium ions enter the S layers, the

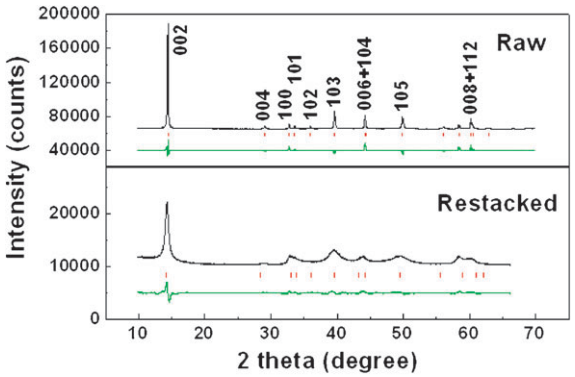

Fig. 2 Rietveld refinement of XRD patterns of raw (top) and restacked (bottom) MoS_2. The observed pattern, the calculated peak positions, and the difference between the observed and the calculated patterns are shown in black, red and green, respectively, from top to bottom.

MoS_2 structure changes from 2H to 1T, namely from trigonal prismatic to octahedral, as illustrated in Fig. S1.† The following MoS_2 decomposition reaction applies:

$$MoS_2 + 4Li \leftrightarrow Mo + 2Li_2S \quad (3)$$

For raw MoS_2, the current at all the peaks decreases with cycling. However, for the restacked sample, the peak at 0.4 V decreases, while the current at the 2.0 V peak increases with cycling, and as a result, a much better cycling performance can be obtained. The cyclic performance curves are in good agreement with the results shown in Fig. 3(c). For raw MoS_2, the charge capacity obviously decreases with the cycle number, from over 800 mAh g^{-1} for the first three cycles to 226 mAh g^{-1} at the 50th cycle. However, the restacked MoS_2 shows much better cycling stability, with a slight decrease after the 40th cycle, which may be caused by electrochemically driven electrolyte degradation over long cycling. After 50 cycles, it still can sustain a high capacity above 750 mAh g^{-1}. The first cycle coulombic efficiency of the raw MoS_2 is 83.5%, and it increases with cycle number, reaching 98% by the 40th cycle. For the restacked MoS_2, the coulombic efficiency of the first cycle is 87.9% and over 98% from the 4th cycle. The rate capability of the restacked MoS_2 electrode was also evaluated at different charge/discharge rates. The restacked MoS_2 displayed extraordinarily high charge storage capacities. The capacities only slightly decrease as the current density increases. The restacked MoS_2 electrodes exhibit a reversible specific capacity as high as 710 mAh g^{-1} at a current density of 1000 mA g^{-1}. It has been reported that for layered structure $LiNi_{0.5}Mn_{0.5}O_2$ cathode material, a small increase in the spacing between Li layers can significantly reduce the activation energy for Li^+ motion.[1] We believe that a similar assumption can also be made for MoS_2 electrodes. The much enlarged *c* parameter, as revealed from Rietveld refinement of the XRD results, relaxes the strain, lowers the barrier for lithium intercalation, and is favorable for Li^+ diffusion. Compared to the raw MoS_2 electrodes, the restacked MoS_2 possesses faster ion conductivity and electrochemical reaction speed under charge/discharge, and therefore shows significantly improved rate capability. The specific surface areas of raw and restacked MoS_2 are 4.89 m^2 g^{-1} and 9.83 m^2 g^{-1}, respectively, so another

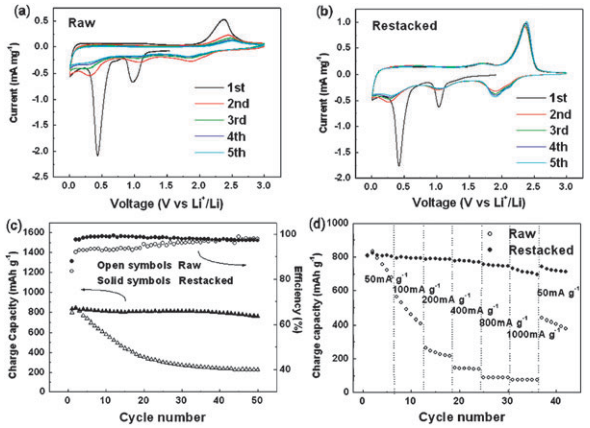

Fig. 3 Electrochemical properties of raw and restacked MoS_2: cyclic voltammograms of (a) raw and (b) restacked MoS_2 at a scanning rate of 0.2 mV s^{-1}; (c) cycling performances at a current density of 50 mA g^{-1}; (d) rate capabilities at different current densities (discharge current density was kept at 50 mA g^{-1}).

possible reason for improved electrochemical performances of restacked MoS_2 is the increase of the surface area, particularly at edges, which would facilitate interfacial reactions. This is also supported by the magnetic measurement results (ESI Fig. S3).† The restacked MoS_2 shows much higher magnetization than the raw MoS_2 due to higher density of edge terminations, in which the different Mo:S coordination generates magnetism.[18]

The restacked MoS_2 electrode after cycling was characterized by TEM and XRD, as shown in ESI Fig. S4.† The reduction of crystallite size of the restacked MoS_2 after cycling, down to about 10 nm, is believed to be due to the electrochemically-driven grinding and size-reduction of the initial particles. The SAED pattern comprises a diffuse set of rings/diffuse bright spots indicating the very small size of crystallites and lattice defects. No obvious peaks can be observed from 10° to 40° in the *ex situ* XRD pattern, consistent with the nanoparticle nature of the electrochemically formed species.[19]

In order to evaluate the effect of the enlarged *c* parameter on reducing the activation energy for Li^+ motion and to understand the electrode kinetics, the apparent activation energies of the raw and restacked MoS_2 were calculated from electrochemical impedance spectra.[20,21] The relevant results are shown in ESI Fig. S5, S6, S7 and Table S1.† The activation energies of the raw and restacked MoS_2 at 1.6 V are calculated to be 68.3 and 63.3 kJ mol^{-1}, respectively. When discharged to 0.9 V, the activation energies are 63.5 and 41.5 kJ mol^{-1}, respectively. The activation energy of the restacked MoS_2 is slightly smaller than that of the raw material at 1.6 V, which means a faster Li diffusion. However at 0.9 V, there is a phase transition from the pristine 2H form to the 1T form when Li intercalates into the S slabs and the molybdenum atoms change from trigonal prismatic coordination to octahedral coordination. The activation energy for the restacked MoS_2 is much smaller than that of the raw materials. This is quite consistent with the previous analysis that the motivation barrier to Li^+ motion is reduced when the space around Li increases and the diffusion length for lithium ions are shortened due to the decrease of the crystallite size, especially for high current charge process.

In summary, we have prepared restacked MoS_2 with an enlarged *c*-axis parameter by exfoliation and then restacking by a simple hydrothermal method. The enlarged *c* parameter and the increase of surface area are favorable to the intercalation reaction, which can also be proven by electrochemical kinetic analysis. The restacked MoS_2 electrodes exhibit a large capacity of 800 mAh g^{-1} and extraordinarily high cycling stability, even at high charge current density. The present results suggest that the restacked MoS_2 is a promising anode material for lithium ion batteries. The strategy, *i.e.* enlarging the space between layers and increasing the surface area (especially edge area) for electrode materials with layered structures, could be a common way to improve the intercalation kinetics in terms of rechargeable batteries.

This work was financially supported by the Australian Research Council (ARC) through an ARC Discovery project (DP0878611). Moreover, the authors would like to thank Dr Tania Silver for critical reading of the manuscript and valuable remarks.

Notes and references

1 K. Kang, Y. S. Meng, J. Breger, C. P. Grey and G. Ceder, *Science*, 2006, **311**, 977.
2 E. Benavente, M. A. Santa Ana, F. Mendizabal and G. Gonzalez, *Coord. Chem. Rev.*, 2002, **224**, 87.
3 F. Wypych and R. Schollhorn, *J. Chem. Soc., Chem. Commun.*, 1992, **19**, 1386.
4 K. D. Bronsema, J. L. de Boer and F. Jellinek, *Z. Anorg. Allg. Chem.*, 1986, **540**, 15.
5 B. Schoenfeld, J. J. Huang and S. C. Moss, *Acta Crystallogr., Sect. B: Struct. Sci.*, 1983, **39**, 404.
6 Q. Wang and J. H. Li, *J. Phys. Chem. C*, 2007, **111**, 1675.
7 J. Chen, Z. L. Tao and S. L. Li, *Angew. Chem., Int. Ed.*, 2003, **42**, 2147.
8 M. S. Whittingham, *Science*, 1976, **192**, 1126.
9 M. A. Santa Ana, V. Sanchez and G. Gonzalez, *Electrochim. Acta*, 1994, **40**, 1773.
10 R. Bissessur and W. White, *Mater. Chem. Phys.*, 2006, **99**, 214.
11 J. Heising and M. G. Kanatzidis, *J. Am. Chem. Soc.*, 1999, **121**, 11720.
12 M. Chhowalla and G. A. J. Amaratunga, *Nature*, 2000, **407**, 164.
13 P. Joensen, R. F. Frindt and S. R. Morrison, *Mater. Res. Bull.*, 1986, **21**, 457.
14 P. Joensen, E. D. Crozier, N. Alberding and R. F. Frindt, *J. Phys. C: Solid State Phys.*, 1987, **20**, 4043.
15 H. Li, W. J. Li, L. Ma, W. X. Chen and J. M. Wang, *J. Alloys Compd.*, 2009, **471**, 442.
16 C. Q. Feng, J. Ma, H. Li, R. Zeng, Z. P. Guo and H. K. Liu, *Mater. Res. Bull.*, 2009, **44**, 1811.
17 M. A. Py and R. R. Haering, *Can. J. Phys.*, 1983, **67**, 76.
18 J. Zhang, J. M. Soon, K. P. Loh, J. H. Yin, J. Ding, M. B. Sullivian and P. Wu, *Nano Lett.*, 2007, **7**, 2370.
19 Y. Sharma, N. Sharma, G. V. Subba Rao and B. V. R. Chowdari, *Adv. Funct. Mater.*, 2007, **17**, 2855.
20 H. Ma, S. Y. Zhang, W. Q. Ji, Z. L. Tao and J. Chen, *J. Am. Chem. Soc.*, 2008, **130**, 5361.
21 S. L. Chou, J. Z. Wang, J. Z. Sun, D. Wexler, M. Forsyth, H. K. Liu, D. R. MacFarlane and S. X. Dou, *Chem. Mater.*, 2008, **20**, 70.

